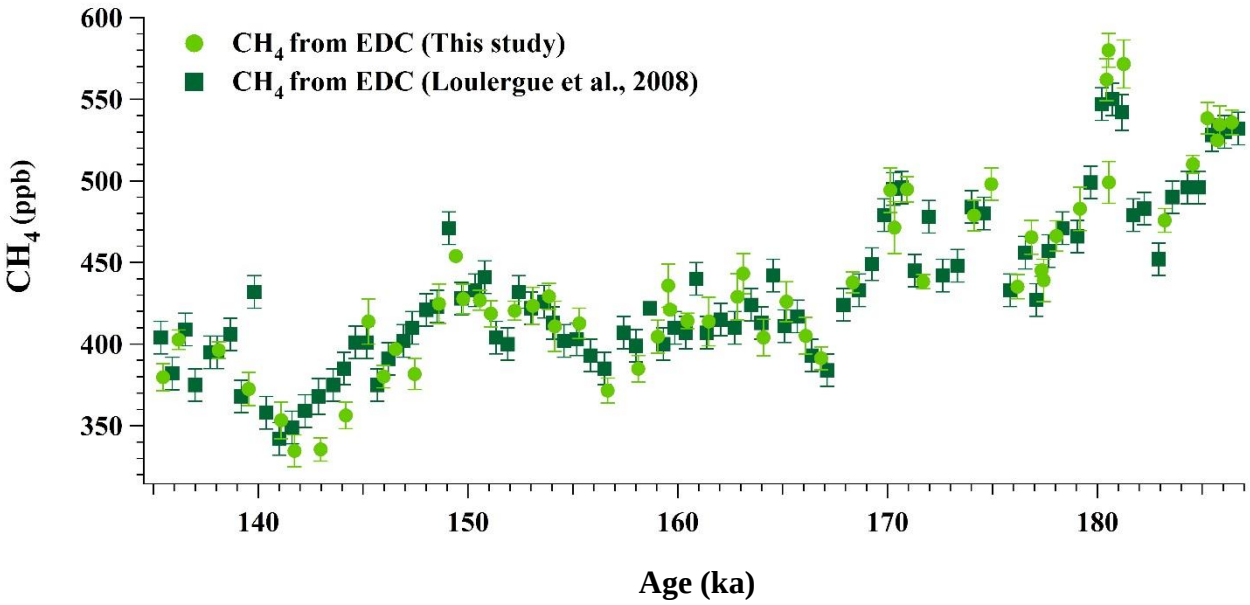

Figure S1. Atmospheric CH_4 concentrations derived from the EPICA Dome C (EDC) ice core covering Marine Isotope Stage (MIS) 6. Dark green squares: published CH_4 data (Loulergue et al., 2008). Light green dots: new CH_4 data (this study). Both data are on the AICC2012 chronology.

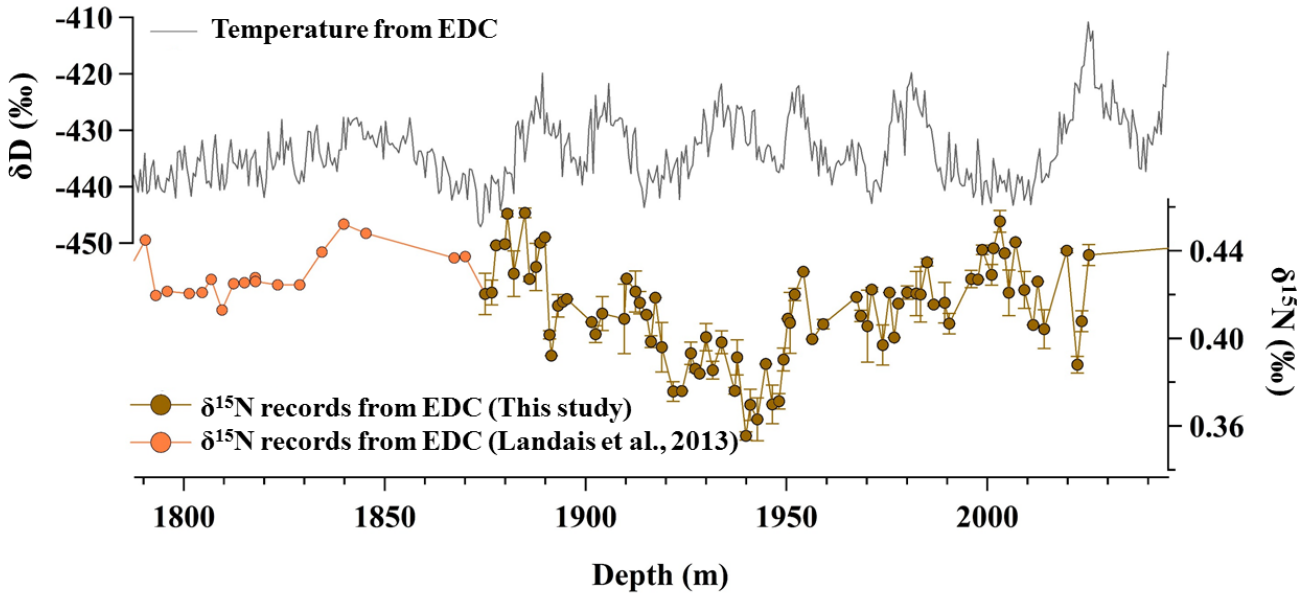

Figure S2. δD (here used as a proxy for Antarctic temperature) (Jouzel et al., 2007) and $\delta^{15}N$ from the EPICA Dome C (EDC) ice core plotted as a function of depth. For $\delta^{15}N$, 88 new data points are added to the previous measurements (Landais et al., 2013). The error bar indicates the standard deviation of duplicate measurements.

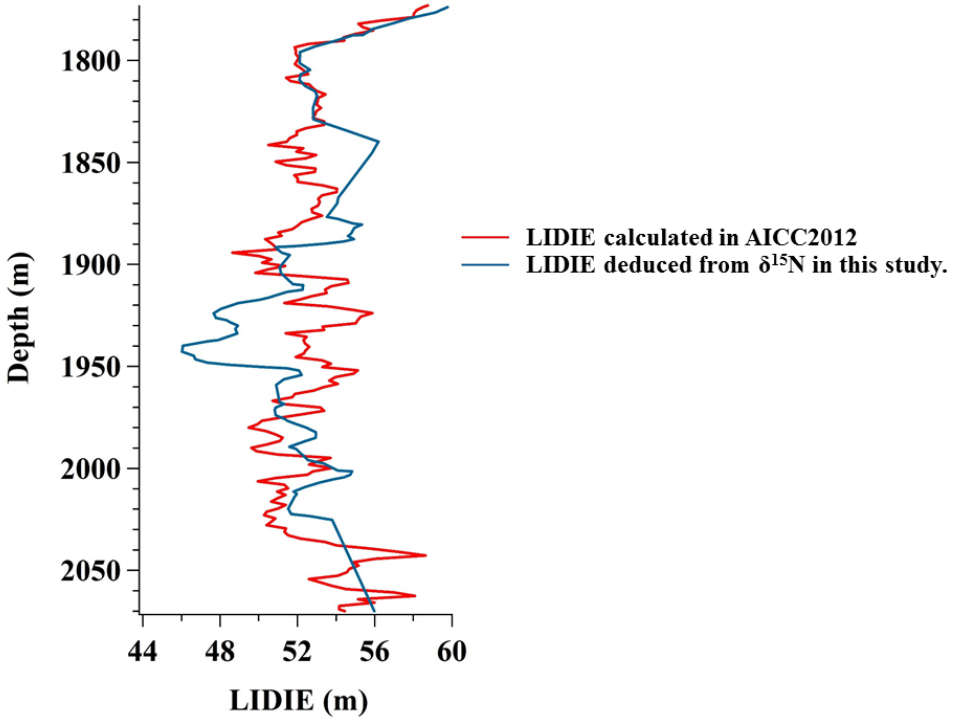

Figure S3. The Lock-In Depth in Ice Equivalent (LIDIE) calculated in the AICC2012 age scale (Bazin et al., 2013) and the LIDIE deduced from $\delta^{15}N$ in this study.

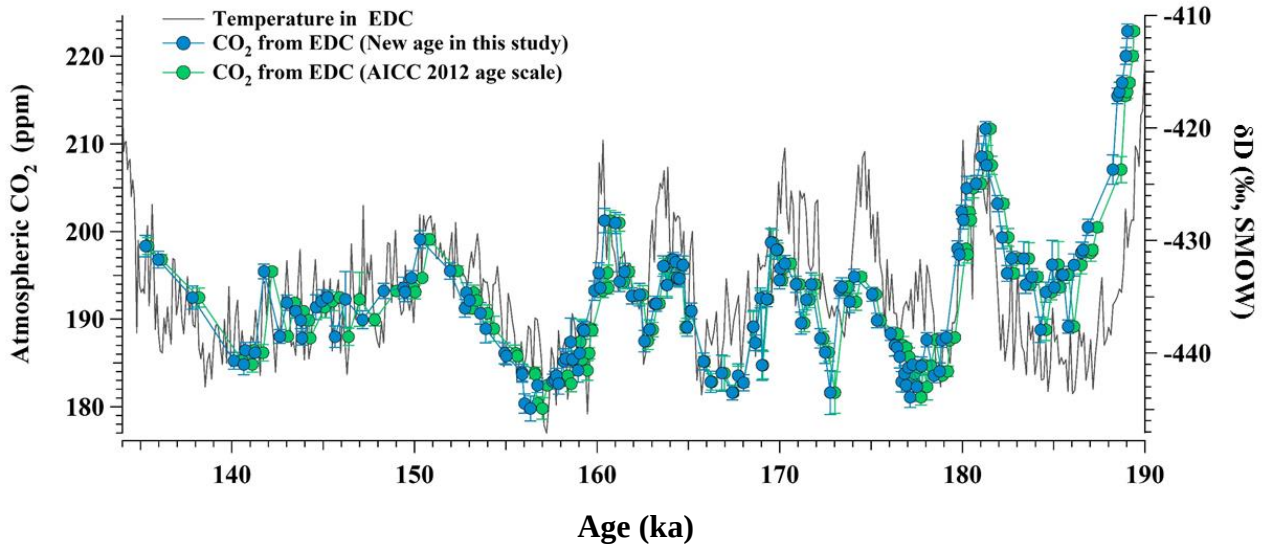

Figure S4. Blue dots: Atmospheric CO_2 measured on the EPICA Dome C (EDC) ice core on the revised age scale (this study). Green dots: Same data on the AICC2012 age scale (Bazin et al. 2013). Grey line: δD of water from EDC (here used as a Antarctic temperature proxy) (Jouzel et al., 2007).

Table S1. Ages of the tie points of MD01–2444 record (Margari et al., 2010) on the EDC03 (Parrenin et al., 2007) and AICC2012 ice age scales (Bazin et al., 2013).

MD01–2444 (m)	Previous age tie points by Margari et al. (2010) (EDC03 age scale, ka)	New age tie points (AICC2012, ka)
22.02	136.100	135.761
22.50	141.686	141.677
23.70	149.586	150.287
24.48	159.105	160.327
24.72	162.476	163.878
25.32	168.273	170.349
25.71	172.009	174.649
25.95	175.461	178.423
26.01	177.065	180.033
27.03	188.009	190.229
27.30	192.231	194.186

Definition of minima and maxima of atmospheric CO_2 and temperature

A two-steps procedure was used in order to select the maxima and minima of temperature during the penultimate glacial periods, and calculate the associated age uncertainty (Figure S5─S6 and Table S2─S3 in SI (Supplement Information)). First, inflection points were selected by finding zero values in the second Savitsky–Golay filtered derivative of the data. The parameters of the Savitsky–Golay filters were chosen in order to remove sub–millennial scale variations that represent noise in the data and are of non-atmospheric orgin. Second, a Monte Carlo-type simulation was conducted, in which the original data were resampled within their uncertainty, and the absolute minima and maxima between pairs of inflection points were selected. This allows us to estimate the uncertainty related to the location of each minimum/maximum. The age uncertainty associated with sampling (taken to be the mean sampling resolution) was added (sum of squares) to the uncertainty calculated in the Monte Carlo procedure to calculate a total uncertainty value.

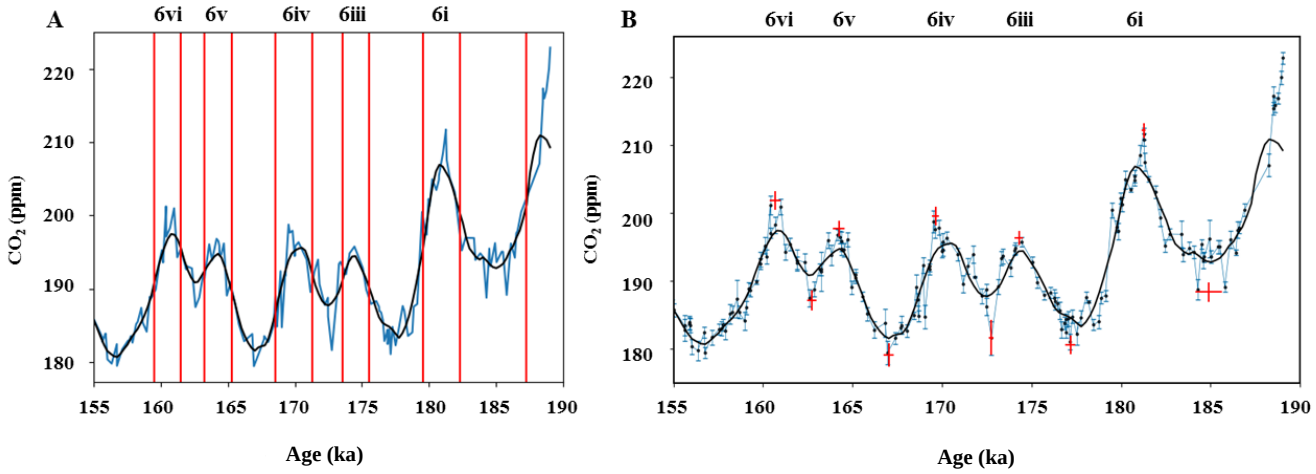

Figure S5. Selecting the maxima and minima of a composite atmospheric CO_2 from the EDC during MIS 6. The black curve in both panels shows the Savitsky-Golay filtered atmospheric CO_2 series. A: Red vertical lines mark inflection points and the blue curve shows the original data. B: Blue dots indicate the composite atmospheric CO_2 data. Red dots indicate the minimum/maximum of Atmospheric CO_2. The error bars indicate the timing and uncertainty for each minimum/maximum. The event numbers are written at the top.

Table S2. The minima and maxima locations of atmospheric CO_2 during the MIS 6.

	CDM 6vi		CDM 6v		CDM 6iv		CDM 6iii		CDM 6i	
	Max	Min	Max	Min	Max	Min	Max	Min	Max	Min
Age (ka)	160.67	162.72	164.23	167.02	169.64	172.75	174.29	177.18	181.26	184.89
2σ (kyr)	0.31	0.26	0.33	0.29	0.19	0.14	0.23	0.28	0.12	0.75

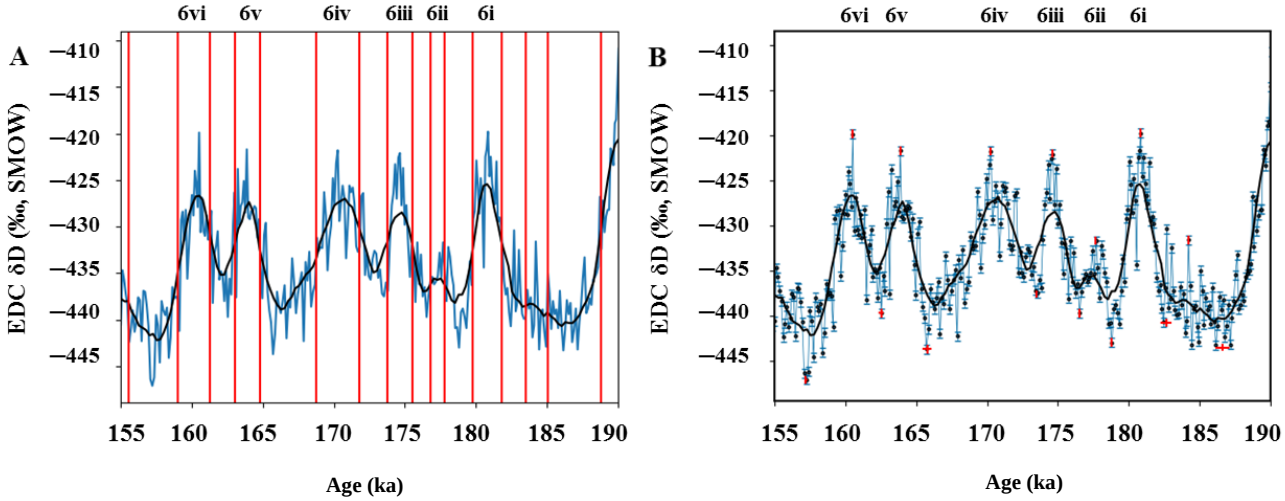

Figure S6. Selecting the maxima and minima of δD from the EDC during MIS 6. The black curve in both panels shows the Savitsky-Golay filtered δD series. A: Red vertical lines mark inflection points and the blue curve shows the original data. B: Blue dots indicate the original data. Red dots are the minimum/maximum of δD. The error bars indicate the timing and δD uncertainty for each minimum/maximum. The event numbers are written at the top.

Table S3. The minima and maxima locations of δD in the EDC during the MIS 6.

	AIM 6vi		AIM 6v		AIM 6iv		AIM 6iii		AIM 6ii		AIM 6i	
	Max	Min	Max	Min	Max	Min	Max	Min	Max	Min	Max	Min
Age (ka)	160.53	162.52	163.88	165.80	170.27	173.49	174.62	176.52	177.67	178.81	180.85	184.61
2σ (kyr)	0.06	0.15	0.06	0.38	0.06	0.09	0.09	0.12	0.08	0.07	0.06	0.62

Table S4. Definition of the duration of each NA stadial using the AICC2012 chronology.

Event name	Definition of NA stadial duration					
	A: Using $\delta^{18}O$ of planktic foraminifera and tree pollen in MD01–2444		B: Using δD in EDC		C: Using the mean of the durations estimated by the methods used for A and B	
	Duration kyr	Uncertainty kyr	Duration kyr	Uncertainty kyr	Duration kyr	Uncertainty kyr
MIS 6vi	1.75	0.29	1.99	0.16	1.87	0.33
MIS 6v	2.77	0.27	1.92	0.38	2.35	0.47
MIS 6iv	3.3	0.23	3.21	0.11	3.26	0.26
MIS 6iii	2.62	0.29	1.90	0.15	2.26	0.33
MIS 6ii	1.1	0.25	1.14	0.10	1.12	0.27
MIS 6i	2.39	0.2	3.76	0.63	3.07	0.66

Table S5. Existing CO_2 data sets from EDC, Vostok ice core and new CO_2 data from EDC during MIS 6.

Ice core	Method (Reference)	CO_2 difference with CO_2 from EDC by ball mill in this study (ppm)	Contamination correction	Gravitational fractionation effect correction	Number of replicates	Number of samples
EDC	Sublimation at CEP Schneider et al. (2013)	4.7± 1.7 (1σ)	yes	This study	2–5	14
	Ball mill at IGE Lourantou et al. (2010)	2.4±2.1 (1σ)	no	Original publication	1	11
	Ring mill at IGE (This study)	8.2±1.1 (1σ)	yes	This study	1	11
	Needle cracker at CEP (This study)	7.8± 1.1 (1σ)	yes	This study	2–4	35
	CIM at CEP (This study)	5.4± 1.0 (1σ)	yes	This study	2–4	26
Vostok	Ball mill at CEP Petit et al. (1999)	4.6± 3.0 (1σ)	no	This study	1	49

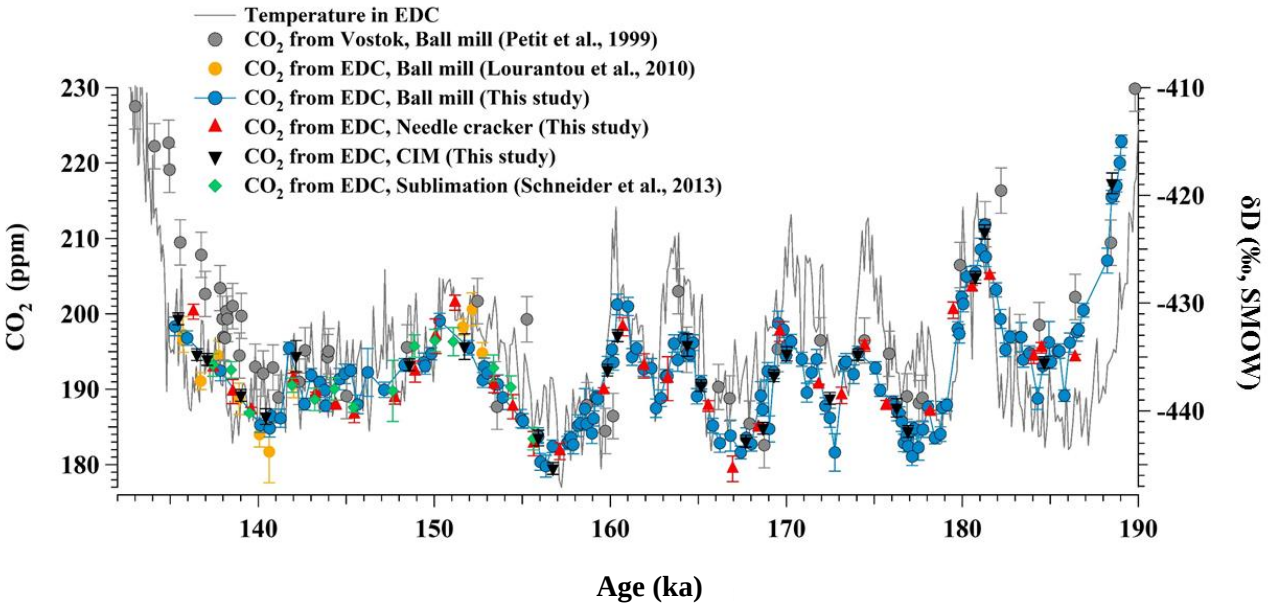

Figure S7. Offset corrected atmospheric CO_2 from EDC (composite) and Vostok ice cores, compared to the δD of water at EDC (temperature proxy) during 190─135 ka. Blue dots: Atmospheric CO_2 from EDC by ball mill system (this study). The error bars of the new CO_2 data using the ball mill extraction system indicate the standard deviation of five consecutive injections of the gas extracted from each sample into the gas chromatograph added to the precision of the measurement estimated by the reproducibility of the control measurement (~0.8 ppm) using a quadratic sum. Yellow dots: Atmospheric CO_2 from EDC by ball mill system (Lourantou et al., 2010). The error bars indicate the standard deviation of five consecutive injections of the gas extracted from each sample into the gas chromatograph. Red equilateral triangles: Atmospheric CO_2 from EDC by needle cracker (this study). The error bars of data points with replicates indicate the standard deviation of the mean of replicates from the same depth interval. Black inverted triangles: Atmospheric CO_2 from EDC by CIM (this study). The error bars of data points with replicates indicate the standard deviation of the mean of replicates from the same depth interval. Green rhombuses: Atmospheric CO_2 from EDC by sublimation (Schneider et al., 2013). The error bars of data points with replicates indicate the standard deviation of the mean of replicates from the same depth interval (Schneider et al., 2013). Grey dots: Atmospheric CO_2 from the Vostok ice core (Petit et al., 1999). The error bars of the CO_2 data from Vostok (Petit et al., 1999) show the estimated overall accuracy for CO_2 measurements. Grey line: δD of water at EDC (Jouzel et al., 2007).

A composite data set during MIS 6

Due to the variety of CO_2 data available for MIS 6 from the EDC ice core, we compiled all data by correcting previously measured (published and unpublished) data to match our new data set. There are two previously published CO_2 data sets available from the EDC ice core during MIS6, one measured at IGE using the ball mill system (Lourantou et al., 2010) and the other at CEP employing a sublimation extraction (Schneider et al., 2013) (Figure 4 and Table S5 in SI). In adddtion, we include unpublished atmospheric CO_2 measurements from the EDC ice core using the needle cracker (Monnin et al., 2004; Siegenthaler et al., 2005) in 2003. All records are on the AICC2012 gas age scale (Bazin et al., 2013). All data sets are corrected for the gravitational fractionation effect using the new $\delta^{15}N$ data in our study.

Because of the limited sample availablitlity, the data reconstructed by the ball mill method are single measurements per depth interval, however, due to the relatively large sample size we thereby integrate over cm-scale CO_2 variability found in the ice core (Lüthi et al., 2010; Schaefer et al., 2011). The error bars of the new CO_2 data using the ball mill extraction system indicate the standard deviation of five consecutive injections of the gas extracted from each sample into the gas chromatograph added to the precision of the measurement estimated by the reproducibility of the control measurement (~0.8 ppm) using a quadratic sum. The error bars of previously published CO_2 data using ball mill without replicates indicate the standard deviation of five consecutive injections of the gas extracted from each sample into the gas chromatography (Lourantou et al., 2010; Petit et al., 1999). CO_2 records made using the CIM, needle cracker and the sublimation method were reconstructed from 2–5 replicates from neighbouring depth sections. The error bars of data with replicates indicate the standard deviation of the mean of replicates from the same depth interval (Schneider et al., 2013).

Figure 4 shows CO_2 concentrations measured by the ball mill system, the sublimation, the CIM and the needle cracker. These CO_2 concentrations by the ball mill system (Lourantou et al., 2010), the sublimation (Schneider et al., 2013), the CIM and the needle cracker are systematically higher than CO_2 concentrations measured by the ball mill system in our study (Table S5 in SI and Figure 4). The estimated offset between the existing CO_2 dataset from EDC by Lourantou et al. (2010) and our new ball mill dataset is ~2.4±2.1 ppm. The CO_2 data from EDC by Lourantou et al. (2010) were also reconstructed using the ball mill system. However, the earlier dataset was not corrected for the CO_2 contamination caused by the analytical procedure. We estimated the level of CO_2 contamination to be between 1 and 2 ppm for our study. Considering that the previous dataset was not corrected, the offset between the two data sets is negligible. Atmospheric CO_2 during the MIS 6 period shows an offset between CO_2 data in this study and other CO_2 sets, which might be related to different analytical methods.

Where the additional datasets have sufficient resolution, the millenial-scale variations shown in our MIS 6 dataset are well reproduced. Nevertheless, the measurements in the different datasets cannot be immediately aggregated because of offsets between their absolute CO_2 values. These offsets do not present any significant temporal evolution over MIS 6, but rather appear to be constant. In order to estimate these offsets while accounting for both measurement uncertainty and uncertainty in the offsets themselves, we rely on a Monte Carlo-type procedure, which is run for 1000 iterations. At each iteration, the data points from all datasets are varied within their measurement uncertainty. Then, a Savitsky-Golay filter with an approximate cutoff period of 150 years (using a 7-point sliding window and cubic fit, sampled at 250-year resolution) is applied to the new

EDC data from this study. The offsets between each additional data set and our data are calculated. At the end of the stochastic procedure, the mean and standard deviation of each offset are calculated, and used to adjust each dataset to create the composite CO_2 dataset (Table S5 and Figure S5 in SI).

In order to test the sensitivity of the stack to the interpolation methods, similiar procedures were also run using linear interpolation, cubic spline filtering, and enting spline filtering instead of the the Savitsky-Golay filter. The mean calculated offsets did not vary by more than 0.2 ppm between different methods, which is well within the uncertainty ranges calculated for the offsets themselves.

There are two main sources of uncertainty in the composite dataset: (i) the measurement uncertainty of the data, and (ii) the uncertainty of the offset itself. Therefore, these two sources of uncertainty are presented separately, and not combined into a single estimate. All calculations using the stack take both sources of uncertainty into account.

We also use this procedure to estimate an offset between our data and the data measured on the Vostok ice core (Table S5 in SI and Figure 4). However, this offset does appear to evolve over time, changing during late MIS 6. Additionally, uncertainties in the alignment of the Vostok and EDC age scales over MIS 6 make it unclear if the variations in the two data series are indeed contemporaneous. We therefore do not include the Vostok data in the composite record.

Offsets between CO_2 records

Atmospheric CO_2 is a well mixed greenhouse gas in the atmosphere and ice-core derived CO_2 reconstructions should therefore agree with each other, at least within the measurement uncertainty. However, small offsets are often found among various different ice cores for different climatic background conditions (Ahn et al., 2012; Bereiter et al., 2012; Marcott et al., 2014). The causes of such offsets often remain elusive. Offset causing mechanisms may alter the CO_2 concentration at any point in time, including in the ice sheet itself (*in-situ* production), during the drilling of the ice core (e.g. by contamination with drilling fluid), while storing the ice (e.g. through gas loss), or during the post-analytic data processing (e.g. data standardization). A comprehensive overview of potential offset causing mechanisms can be found in Bereiter et al. (2012) and Eggleston et al. (2016).

Most offset causing mechansims lead to an increase in the measured CO_2 concentration, i.e. CO_2 is added at some stage. The only plausible mechanisms that could explain lower values are the way the measurement signal is converted into a mole fraction (calibration and standardization) or gas extraction methodologies. The most likey explanation mayinvolve ice relaxation (clathrate decay) during the long storage period (Bereiter et al., 2015) and the choice of extraction device.

During clathrate formation, the gas is partitioned into clathrates due to the different gas diffusivities and solubilities (Salamatin et al., 2001). CO_2 has consistently been observed to be depleted in bubbles and enriched in clathrates (Schaefer et al., 2011). Degassing from clathrates during extraction takes much longer than air release from bubbles; thus, if air from the clathrate ice is not extracted entirely, CO_2 measurement will be lower than the true value.

The ball mill shows extraction efficiencies of ~62% for bubbles and ~52% for clathrates on average (Schaefer et al., 2011). If the ball mill is used to reconstruct CO_2 in Bubble–Clathrate Transformation Zone (BTCZ), CO_2 concentrations can be biased. CO_2 concentrations from EDC were reconstructed from 177 depth intervals that cover 2036.7 to 1787.5 m along the EDC ice core, which consist of clathrate ice. There exists true small scale variability in CO_2 concentrations in the ice below the Clathrate Zone (Lüthi et al., 2010). Due to slow bubble formation, this small variation of atmospheric CO_2 is smoothed. Thus, CO_2 concentrations in these depth intervals should represent the initial mean atmospheric concentration. However, the EDC ice core had been stored for ~20 years in cold rooms at -22.5 ± 2.5°C before the gas was analysed. More than 50% of the initial hydrates present in the freshly drilled ice may have been decomposed and transformed into secondary bubbles, or gas cavities (Lipenkov, *Pers. Comm.*). We expect the same fractionation as during the clathrate formation process, hence bubbles would be depleted in CO_2. Thus, CO_2 concentrations from EDC may be lower. The portion of the Vostok ice core covering MIS 6 is also clathrate ice, but it was measured not long after drilling (Petit et al., 1999), and less clathrates may have transformed into secondary bubbles. Thus CO_2 concentrations from Vostok during MIS 6 may be higher and potentially reflect the true atmospheric concentration more closely. In our study we concentrate on the relative millennial changes of CO_2 around the mean glacial concentration, which are the same in all the CO_2 records available so far, Thus, our conclusion in this paper are independent of which absolute mean CO_2 level is correct. As the new data in this study are currently the best quality data in terms of repeatability, we use this data as the reference record for the correction of all remaining records. We stress that the absolute mean CO_2 level during MIS6 is not known better than 5 ppm.

Definition of the onset of abrupt climate change in the NH

Over the last glacial period, rapid CH_4 rises are synchronous with abrupt temperature increases in Greenland within ±50 ppb (Huber et al., 2006) and may even occur simultaneously (Rosen et al., 2014). Here, we choose intervals of rapid CH_4 increases greater than 50 ppb over a time period of less than 1 kyr that correspond with Antarctic Isotope Maxima (EPICA Community Members, 2006; Loulergue et al., 2008). The timing of abrupt CH_4 increases was defined as the midpoint between the beginning of the increase of CH_4 and its maximum The age uncertainty of the midpoint is defined by the time difference between the midpoint and either of the two endpoints (cf. Bereiter et al. 2012).

We found three abrupt CH_4 increases during MIS 6 at 171.1±0.2, 175.4±0.4 and 181.5±0.3 ka (Figure S8 in SI). Due to the low accumulation rate and low temperature at the site during glacial periods, abrupt changes of CH_4 concentration might be smoothed, and identifying abrupt changes of CH_4 is more difficult than for interglacial periods. The climate change at 175.4 ka does not seem to occur as abruptly as the other two, since CH_4 varied slowly over ~800 years. However, we include this event because corresponding data of $\delta^{18}O$ composition of planktonic foraminifera (Shackleton et al., 2000) indicate a rapid warming, and therefore an abrupt climate change in NH (Figure 3). Rapid increases during the last glacial period (MIS 3 and 5) are also calculated using this method to identify the onset of abrupt warming in NH. In total, eight abrupt rises are selected during this period (Figure S8–S11 in SI).

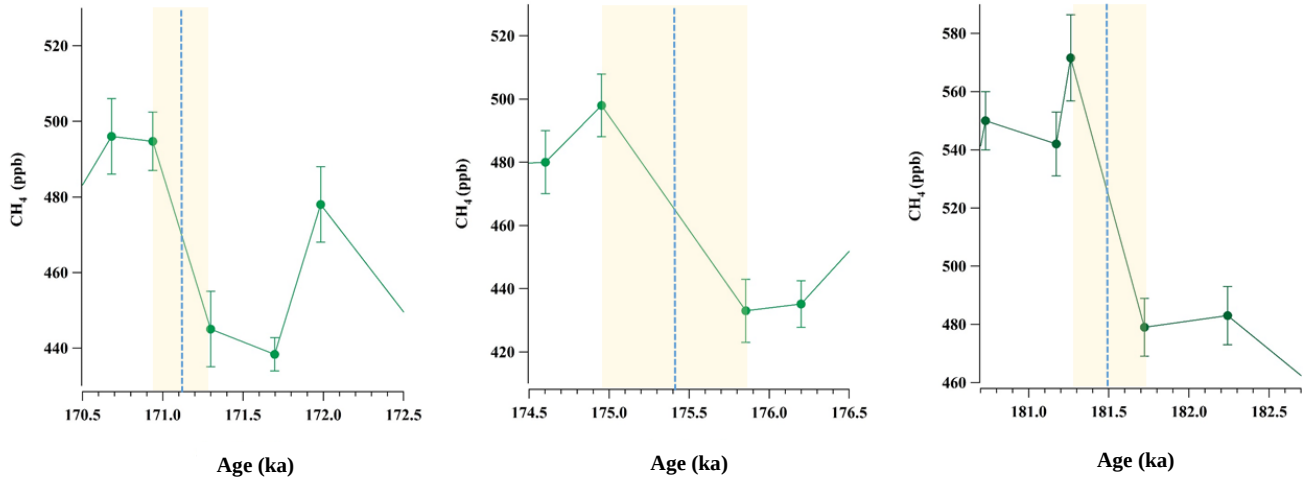

Figure S8. Atmospheric CH_4 records from EDC during MIS 6 period. Three boxes show CH_4 jumps at 171.1±0.2, 175.4 ±0.4 and 181.5±0.3 ka.

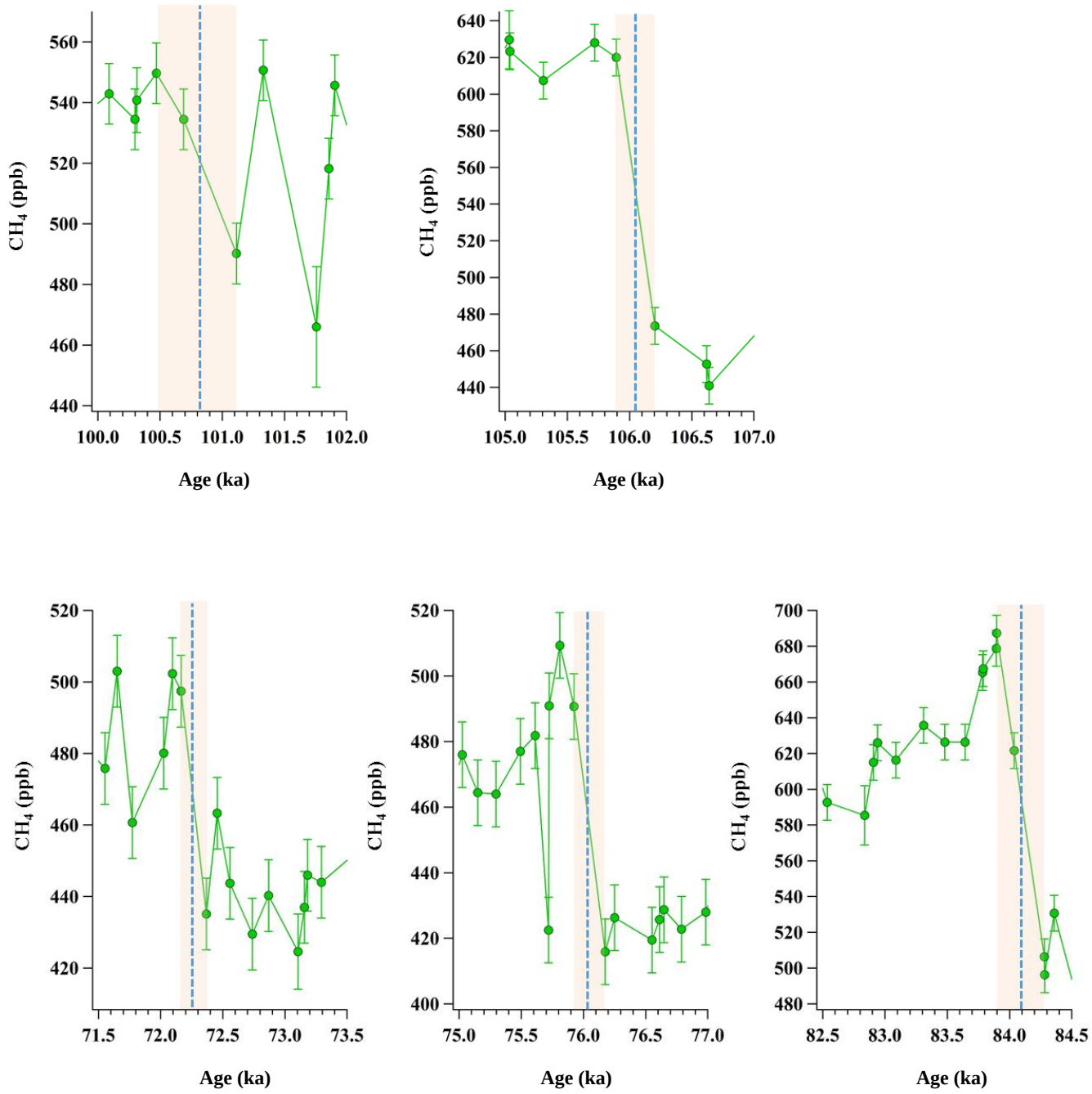

Figure S9. Atmospheric CH_4 records from EDML during the MIS 5 period. Five boxes show CH_4 jumps at 72.3±0.1, 76.0±0.1, 84.1±0.2, 100.8±0.5 and 106.0±0.2 ka.

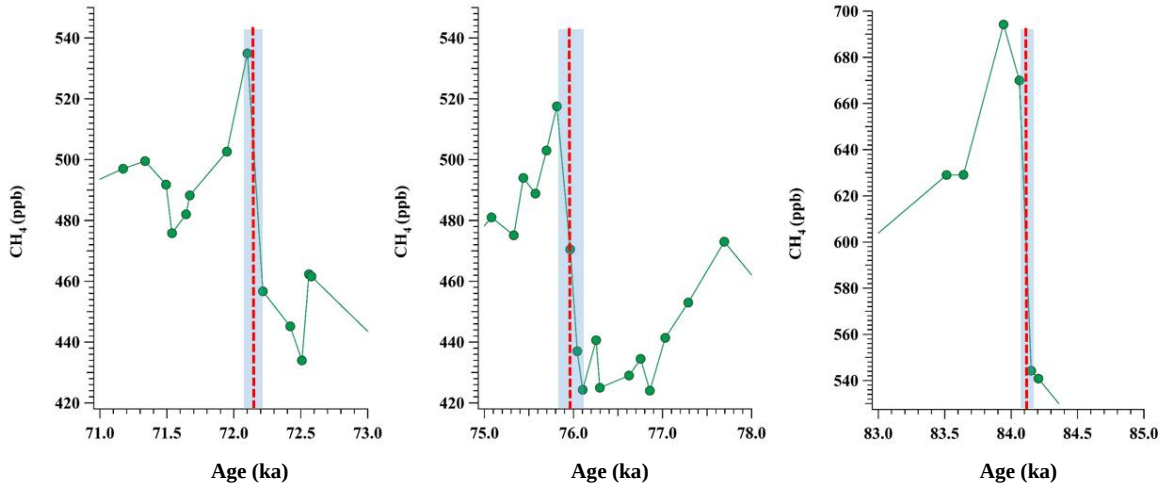

Figure S10. Atmospheric CH_4 records from the Byrd ice core during MIS 5 period. Three boxes show CH_4 jumps at 72.2±0.1, 76.0±0.2 and 84.1±0.04 ka.

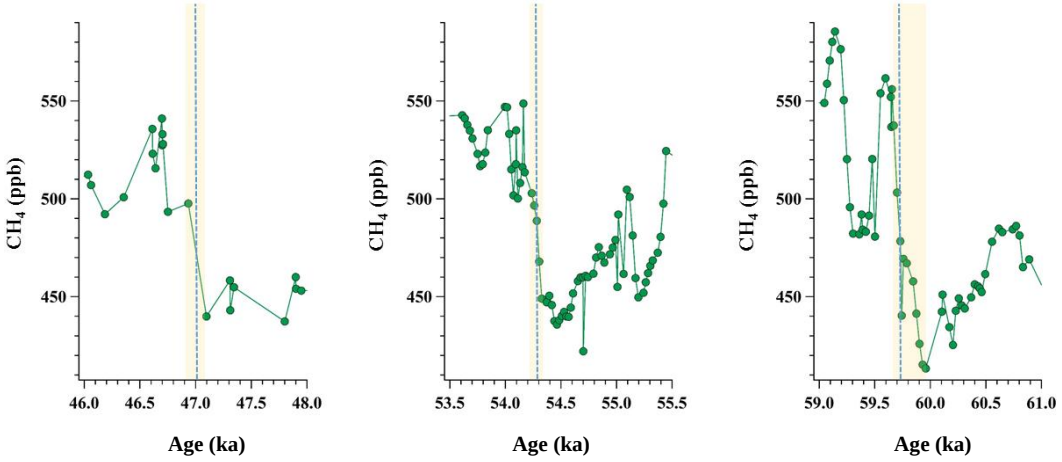

Figure S11. Atmospheric CH_4 records from TALDICE during MIS 3 period. Three boxes show CH_4 jumps at 46.7±0.2, 54.2±0.1 and 59.7±0.1 ka.

References

Ahn, J., Brook, E. J., Mitchell, L., Rosen, J., McConnell, J. R., Taylor, K., Etheridge, D., and Rubino, M.: Atmospheric CO_2 over the last 1000 years: A high-resolution record from the West Antarctic Ice Sheet (WAIS) Divide ice core, Global Biogeochem. Cycles, 26, GB2027, https://doi.org/10.1029/2011GB004247, 2012.

Bazin, L., Landais, A., Lemieux-Dudon, B., Kele, H. T. M., Veres, D., Parrenin, F., Martinerie, P., Ritz, C., Capron, E., and Lipenkov, V.: An optimized multi-proxy, multi-site Antarctic ice and gas orbital chronology (AICC2012): 120-800 ka, Clim. Past, 9, 1715–1731, https://doi.org/10.5194/cp-9-1715-2013, 2013.

Bereiter, B., Eggleston, S., Schmitt, J., Nehrbass-Ahles, C., Stocker, T. F., Fischer, H., Kipfstuhl, S., and Chappellaz, J.: Revision of the EPICA Dome C CO_2 record from 800 to 600 kyr before present, Geophys. Res. Lett., 42, 542-549, doi:10.1002/2014GL061957, 2015.

Bereiter, B., Lüthi, D., Siegrist, M., Schüpbach, S., Stocker, T. F., and Fischer, H.: Mode change of millennial CO_2 variability during the last glacial cycle associated with a bipolar marine carbon seesaw, Proc. Natl. Acad. Sci., 109, 9755-9760, doi:10.1073/pnas.1204069109, 2012.

Eggleston, S., Schmitt, J., Bereiter, B., Schneider, R., and Fischer, H.: Evolution of the stable carbon isotope composition of atmospheric CO_2 over the last glacial cycle, Paleoceanography, 31, 434-452, https://doi.org/10.1002/2015PA002874, 2016.

EPICA Community Members: One-to-one coupling of glacial climate variability in Greenland and Antarctica, Nature, 444, 195-198, doi:10.1038/nature05301, 2006.

Jouzel, J., Masson-Delmotte, V., Cattani, O., Dreyfus, G., Falourd, S., Hoffmann, G., Minster, B., Nouet, J., Barnola, J.-M., and Chappellaz, J.: Orbital and millennial Antarctic climate variability over the past 800,000 years, Science, 317, 793-796, doi:10.1126/science.1141038, 2007.

Landais, A., Dreyfus, G., Capron, E., Jouzel, J., Masson-Delmotte, V., Roche, D. M., Prié, F., Caillon, N., Chappellaz, J., Leuenberger, M., Lourantou, A., Parrenin, F., Raynaud, D., and Teste,G.: Two-phase change in CO_2, Antarctic temperature and global climate during Termination II, Nat. Geosci., 6, 1062–1065, https://doi.org/10.1038/ngeo1985, 2013.

Loulergue, L., Schilt, A., Spahni, R., Masson-Delmotte, V., Blunier, T., Lemieux, B., Barnola, J.-M., Raynaud, D., Stocker, T. F., and Chappellaz, J.: Orbital and millennial-scale features of atmospheric CH_4 over the past 800,000 years, Nature, 453, 383–386, doi:10.1038/nature06950, 2008

Lüthi, D., Bereiter, B., Stauffer, B., Winkler, R., Schwander, J., Kindler, P., Leuenberger, M., Kipfstuhl, S., Capron, E., and Landais, A.: CO_2 and O_2/N_2 variations in and just below the bubble–clathrate transformation zone of Antarctic ice cores, Earth Planet. Sci. Lett., 297, 1–2, 226–233, https://doi.org/10.1016/j.epsl.2010.06.023, 2010.

Marcott, S. A., Bauska, T. K., Buizert, C., Steig, E. J., Rosen, J. L., Cuffey, K. M., Fudge, T. J., Severinghaus, J. P., Ahn, J., Kalk, M. L., McConnell, J. R., Sowers, T., Taylor, K. C., White, J. W., and Brook, E. J.: Centennial scale changes in the global carbon cycle during the last deglaciation, Nature, 514, 616–619, doi:10.1038/nature13799, 2014.

Margari, V., Skinner, L., Tzedakis, P., Ganopolski, A., Vautravers, M., and Shackleton, N.: The nature of millennial-scale climate variability during the past two glacial periods, Nat.Geosci., 3, 127–131, https://doi.org/10.1038/ngeo740, 2010.

Monnin, E., Steig, E. J., Siegenthaler, U., Kawamura, K., Schwander, J., Stauffer, B., Stocker, T. F., Morse, D. C., Barnola, J.-M., Bellier, B., Raynaud, D., and Fischer, H.: Evidence for substantial accumulation rate variability in Antarctica during the Holocene through synchronization of CO_2 in the Taylor Dome, Dome C and DML ice cores, Earth Planet. Sc. Lett., 224, 45–54, 2004

Parrenin, F., Barnola, J.-M., Beer, J., Blunier, T., Castellano, E., Chappellaz, J., Dreyfus, G., Fischer, H., Fujita, S., Jouzel, J., Kawamura, K., Lemieux-Dudon, B., Loulergue, L., MassonDelmotte, V., Narcisi, B., Petit, J.-R., Raisbeck, G., Raynaud, D., Ruth, U., Schwander, J., Severi, M., Spahni, R., Steffensen, J. P.,Svensson, A., Udisti, R., Waelbroeck, C., and Wolff, E.: The EDC3 chronology for the EPICA Dome C ice core, Clim. Past, 3, 485–497, doi:10.5194/cp-3-485-2007, 2007.

Petit, J. R., Jouzel, J., Raynaud, D., Barkov, N. I., Barnola, J.-M., Basile, I., Bender, M., Chapellaz, J., Davis, M., Delaygue, G., Delmotte, M., Kotlyakov, V. M., Legrand, M., Lipenkov, V. Y., Lorius, C., Pepin, L., Ritz, C., Saltzmann, E., and

Stievenard, M.: Climate and atmospheric history of the past 420000 years from the Vostok ice core, Antarctica, Nature, 399, 429–436, https://doi.org/10.1038/20859, 1999.

Railsback, L. B., Gibbard, P. L., Head, M. J., Voarintsoa, N. R. G., and Toucanne, S.: An optimized scheme of lettered marine isotope substages for the last 1.0 million years, and the climatostratigraphic nature of isotope stages and substages, Quaternary Sci.Rev., 111, 94–106, 2015.

Rosen, J. L., Brook, E. J., Severinghaus, J. P., Blunier, T., Mitchell, L. E., Lee, J. E., Edwards, J. S., and Gkinis, V.: An ice core record of near-synchronous global climate changes at the Bølling transition, Nat. Geosci., 7, 459–463, https://doi.org/10.1038/ngeo2147, 2014.

Schaefer, H., Lourantou, A., Chappellaz, J., Lüthi, D., Bereiter, B., and Barnola, J.-M.: On the suitability of partially clathrated ice for analysis of concentration and $\delta^{13}C$ of palaeo-atmospheric CO_2, Earth Planet. Sci. Lett., 307, 334-340, https://doi.org/10.1016/j.epsl.2011.05.007, 2011.

Shackleton, N. J., Hall, M. A., and Vincent, E.: Phase relationships between millennial-scale events 64,000–24,000 years ago, Paleoceanography, 15(6), 565-569, doi:10.1029/2000PA000513, 2000.

Siegenthaler, U., Stocker, T. F., Monnin, E., Lüthi, D., Schwander, J., Stauffer, B., Raynaud, D., Barnola, J.-M., Fischer, H., and Masson-Delmotte, V.: Stable carbon cycle–climate relationship during the late Pleistocene, Science, 310, 1313-1317, doi: 10.1126/science.1120130, 2005.